

UNIVERSALITY AND INTERMITTENCY IN RELATIVISTIC TURBULENT FLOWS OF A HOT PLASMA

DAVID RADICE

Max-Planck-Institut für Gravitationsphysik, Albert Einstein Institut, Potsdam, Germany

LUCIANO REZZOLLA

Max-Planck-Institut für Gravitationsphysik, Albert Einstein Institut, Potsdam, Germany and
Department of Physics and Astronomy, Louisiana State University, Baton Rouge, USA

Draft version December 3, 2024

Abstract

With the aim of determining the statistical properties of relativistic turbulence and unveiling novel and non-classical features, we present the results of direct numerical simulations of driven turbulence in an ultrarelativistic hot plasma using high-order numerical schemes. We study the statistical properties of flows with average Mach number ranging from ~ 0.4 to ~ 1.7 and with average Lorentz factors up to ~ 1.7 . We find that flow quantities, such as the energy density or the local Lorentz factor, show large spatial variance even in the sub-sonic case as compressibility is enhanced by relativistic effects. The velocity field is highly intermittent, but its power-spectrum is found to be in good agreement with the predictions of the classical theory of Kolmogorov. Overall, our results indicate that relativistic effects are able to significantly enhance the intermittency of the flow and affect the high-order statistics of the velocity field, while leaving unchanged the low-order statistics, which instead appear to be universal and in good agreement with the classical Kolmogorov theory. To the best of our knowledge, these are the most accurate simulations of driven relativistic turbulence to date.

Subject headings: Relativistic Hydrodynamics, Turbulence

1. INTRODUCTION.

Turbulence is an ubiquitous phenomenon in nature as it plays a fundamental role in shaping the dynamics of systems ranging from the mixture of air and oil in a car engine, up to the rarefied hot plasma composing the intergalactic medium. Relativistic hydrodynamics is a fundamental ingredient in the modeling of a number of systems characterized by high Lorentz-factor flows, strong gravity or relativistic temperatures. Examples include the early Universe, relativistic jets, gamma-ray-bursts (GRBs), relativistic heavy-ion collisions and core-collapse supernovae (Font 2008).

Despite the importance of relativistic hydrodynamics and the reasonable expectation that turbulence is likely to play an important role in many of the systems mentioned above, extremely little is known about turbulence in a relativistic regime. For this reason, the study of relativistic turbulence may be of fundamental importance to develop a quantitative description of many astrophysical systems. To this aim, we have performed a series of high-order direct numerical simulations of driven relativistic turbulence of a hot plasma.

2. MODEL AND METHOD.

We consider an idealized model of an ultrarelativistic fluid with four-velocity $u^\mu = W(1, v^i)$, where $W \equiv (1 - v_i v^i)^{-1/2}$ is the Lorentz factor and v^i is the three-velocity in units where $c = 1$. The fluid is modeled as perfect and described by the stress-energy tensor

$$T_{\mu\nu} = (\rho + p)u_\mu u_\nu + p g_{\mu\nu}, \quad (1)$$

where ρ is the (local-rest-frame) energy density, p is the pressure, u_μ the four-velocity, and $g_{\mu\nu}$ is the spacetime metric, which we take to be the Minkowski one. We evolve the equations describing conservation of energy and momentum

in the presence of an externally imposed Minkowskian force F^μ , i.e. $\nabla_\nu T^{\mu\nu} = F^\mu$, where the forcing term is written as $F^\mu = \tilde{F}(0, f^i)$. More specifically, the spatial part of the force, f^i , is a zero-average, solenoidal, random, vector field with a spectral distribution which has compact support in the low wavenumber part of the Fourier spectrum. Moreover, f^i , is kept fixed during the evolution and it is the same for all the models, while \tilde{F} is either a constant or a simple function of time (see below for details).

The time component of the forcing term, F^0 , is zero, so that the driving force is able to accelerate fluid elements without changing their total energy (in the Eulerian frame). On the other hand, we impose a minimum value for the energy density in the local-rest-frame, ρ_{\min} . This choice is motivated essentially by numerical reasons (the very large Lorentz factor produced can lead to unphysical point-wise values of ρ) and has the effect of slowly heating up the fluid. Furthermore, this floor does not affect the momentum of the fluid and only the temperature is increased. From a physical point of view, our approach mimics the fact that in the low-density regions, the constituents of the plasma are easily accelerated to very high Lorentz factors, hence emitting bremsstrahlung radiation heating up the surrounding regions. The net effect is that energy is subtracted from the driving force and converted into thermal energy of the fluid, heating it up. In general ρ_{\min} is chosen to be two orders of magnitude smaller than the initial energy density, but we have verified that the results presented here are insensitive to the specific value chosen for ρ_{\min} by performing simulations where the floor value is changed by up to two orders of magnitude without significant differences.

The set of relativistic-hydrodynamic equations is closed by the equation of state (EOS) $p = \frac{1}{3}\rho$, thus modelling a hot, optically-thick, radiation-pressure dominated plasma, such as the electron-positron plasma in a GRB fireball or the matter in the radiation-dominated era of the early Universe. The EOS

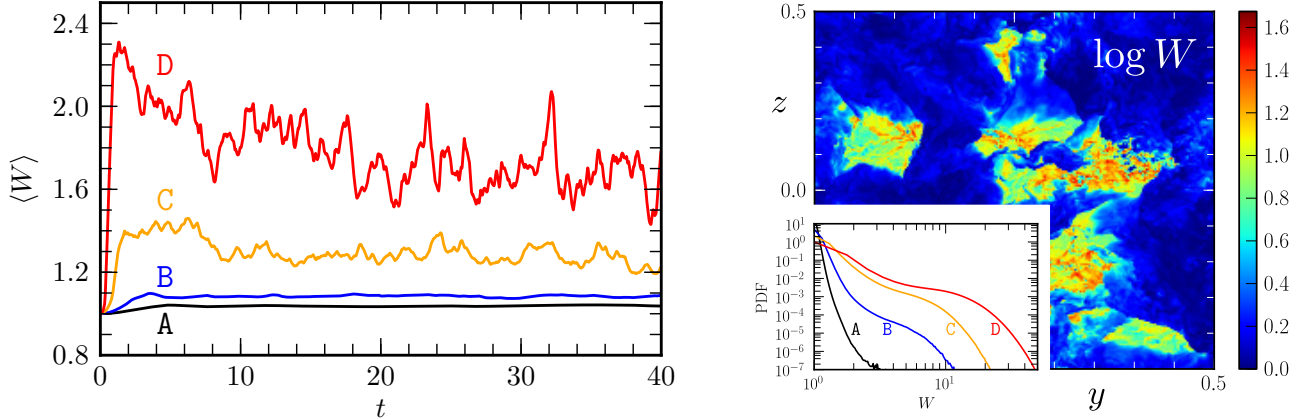


Figure 1. *Left panel:* average Lorentz factor as a function of time for the different models considered. Note that a quasi-stationary state is reached before $t \sim 10$ for all values of the driving force. *Right panel:* logarithm of the Lorentz factor on the (y, z) plane at the final time of model D. Note the large spatial variations of the Lorentz factor with front-like structures. The time-averaged PDFs are shown in the lower left corner for the different models considered.

used can be thought as the relativistic equivalent of the classical isothermal EOS in that the sound speed is a constant, *i.e.* $c_s^2 = 1/3$. At the same time, an ultrarelativistic fluid is fundamentally different from a classical isothermal fluid. For instance, its “inertia” is entirely determined by the temperature and the notion of rest-mass density is lost since the latter is minute (or zero for a pure photon gas) when compared with the internal one. For these reasons, there is no direct classical counterpart of an ultrarelativistic fluid and a relativistic description is needed even for small velocities.

We solve the equations of relativistic hydrodynamics in a 3D periodic domain using the high-resolution shock capturing scheme described in (Radice & Rezzolla 2012). In particular, ours is a flux-vector-splitting scheme (Toro 1999), using the fifth-order MP5 reconstruction (Suresh & Huynh 1997), in local characteristic variables (Hawke 2001), with a linearized flux-split algorithm with entropy and carbuncle fix (Radice & Rezzolla 2012).

3. BASIC FLOW PROPERTIES.

Our analysis is based on the study of four different models, which we label as A, B, C and D, and which differ for the initial amplitude of the driving factor $\tilde{F} = 1, 2, 5$ for models A–C, and $\tilde{F}(t) = 10 + \frac{1}{2}t$ for the extreme model D. Each model was evolved using three different uniform resolutions of 128^3 , 256^3 and 512^3 grid zones over the same unit length-scale. As a result, model A is subsonic, model B is transonic and models C and D are instead supersonic. The spatial and time-averaged relativistic Mach numbers $\langle vW \rangle / (c_s W_s)$ are 0.362, 0.543, 1.003 and 1.759 for our models A, B, C and D, while the average Lorentz factors are 1.038, 1.085, 1.278 and 1.732 respectively.

The initial conditions are simple: a constant energy density and a zero-velocity field. The forcing term, which is enabled at time $t = 0$, quickly accelerates the fluid, which becomes turbulent. By the time when we start to sample the data, *i.e.* at $t = 10$ (light-)crossing times, turbulence is fully developed and the flow has reached a stationary state. The evolution is then carried out up to time $t = 40$, thus providing data for 15, equally-spaced timeslices over 30 crossing times. As a representative indicator of the dynamics of the system, we show in the left panel of Fig. 1 the time evolution of the average Lorentz factor for the different models considered. Note that the Lorentz factor grows very rapidly during the first few crossing times and then settles to a quasi-stationary evolution.

Furthermore, the average grows nonlinearly with the increase of the driving term, going from $\langle W \rangle \simeq 1.04$ for the subsonic model A, up to $\langle W \rangle \simeq 1.73$ for the most supersonic model D.

Flow quantities such as the energy density, the Mach number or the Lorentz factor show large spatial variance, even in our subsonic model. Similar deviations from the average mass density, have been reported also in classical turbulent flows of weakly compressible fluids (Benzi et al. 2008), where it was noticed that compressible effects, leading to the formation of front-like structures in the density and entropy fields, cannot be neglected even at low Mach numbers. In the same way, relativistic effects in the kinematics of the fluid, such those due to nonlinear couplings via the Lorentz factor (Rezzolla & Zanotti 2002), have to be taken into account even when the average Lorentz factor is small. The probability distribution functions (PDFs) of the Lorentz factor are shown in the right panel of Fig. 1 for the different models. Clearly, as the forcing is increased, the distribution widens, reaching Lorentz factors as large as $W \simeq 40$ (*i.e.* to speeds $v \simeq 0.9997$). Even in the most “classical” case A, the flow shows patches of fluid moving at ultrarelativistic speeds. Also shown in Fig. 1 is the logarithm of the Lorentz factor on the (y, z) plane and at $t = 40$ for model D, highlighting the large spatial variations of W and the formation of front-like structures.

4. UNIVERSALITY.

As customary in studies of turbulence, we have analyzed the power spectrum of the velocity field

$$E_v(k) \equiv \frac{1}{2} \int_{|\mathbf{k}|=k} |\hat{\mathbf{v}}(\mathbf{k})|^2 d\mathbf{k}, \quad (2)$$

where \mathbf{k} is a wavenumber three-vector and

$$\hat{\mathbf{v}}(\mathbf{k}) \equiv \int_V \mathbf{v}(\mathbf{x}) e^{-2\pi i \mathbf{k} \cdot \mathbf{x}} d\mathbf{x}, \quad (3)$$

with V being the three-volume of our computational domain. A number of recent studies have analyzed the scaling of the velocity power spectrum in the inertial range, that is, in the range in wavenumbers between the lengthscale of the problem and the scale at which dissipation dominates. More specifically, Inoue et al. (2011) has reported evidences of a Kolmogorov $k^{-5/3}$ scaling in a freely-decaying MHD turbulence, but has not provided a systematic convergence study of the spectrum. Evidences for a $k^{-5/3}$ scaling were also

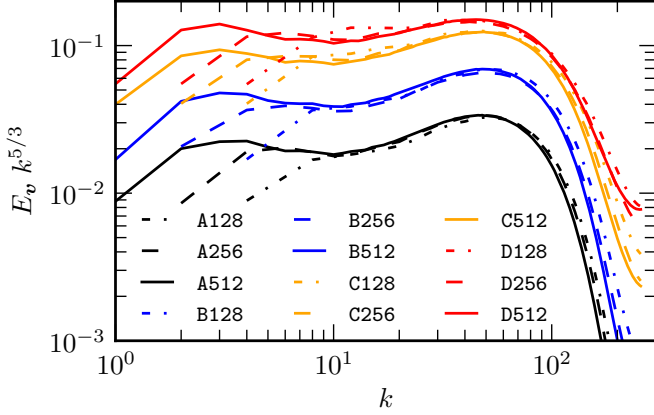


Figure 2. Power spectra of the velocity field. Different lines refer to the three resolutions used and to the different values of the driving force. The spectra are scaled assuming a $k^{-5/3}$ law.

found by Zhang et al. (2009), in the case of the kinetic-energy spectrum, which coincides with the velocity power-spectrum in the incompressible case. Finally, Zrake & MacFadyen (2012) has performed a significantly more systematic study for driven, transonic, MHD turbulence, but obtained only a very small (if any) coverage of the inertial range.

The time-averaged velocity power spectra computed from our simulations are shown in Fig. 2. Different lines refer to the three different resolutions used, 128^3 (dash-dotted), 256^3 (dashed) and 512^3 (solid lines), and to the different values of the driving force. To highlight the presence and extension of the inertial range, the spectra are scaled assuming a $k^{-5/3}$ law, with curves at different resolutions shifted of a factor two or four, and nicely overlapping with the high-resolution one in the dissipation region. Overall, Fig. 2 convincingly demonstrates the good statistical convergence of our code and gives a strong support to the idea that the *key* prediction of the Kolmogorov model (K41) (Kolmogorov 1991) carries over to the relativistic case. Indeed, not only does the velocity spectrum for our subsonic model A shows a region, of about a decade in length, where the $k^{-5/3}$ scaling holds, but this continues to be the case even as we increase the forcing and enter the regime of relativistic supersonic turbulence with model D. In this transition, the velocity spectrum in the inertial range, the range of lengthscales where the flow is scale-invariant, is simply “shifted upwards” in a self-similar way, with a progressive flattening of the bottleneck region, the bump in the spectrum due to the non-linear dissipation introduced by our numerical scheme. Steeper scalings, such as the Burger one, k^{-2} , are also clearly incompatible with our data.

All in all, this is one of our main results: the velocity power spectrum in the inertial range is *universal*, that is, insensitive to relativistic effects, at least in the subsonic and mildly supersonic cases. Note that this does *not* mean that relativistic effects are absent or can be neglected when modelling relativistic turbulent flows.

5. INTERMITTENCY.

Not all of the information about relativistic turbulent flows is contained in the velocity power spectrum. Particularly important in a relativistic context is the intermittency of the velocity field, that is, the local appearance of anomalous, short-lived flow features, which we have studied by looking at the parallel-structure functions of order p

$$S_p^{\parallel}(r) \equiv \langle |\delta_r v|^p \rangle, \quad \delta_r v = [\mathbf{v}(\mathbf{x} + \mathbf{r}) - \mathbf{v}(\mathbf{x})] \cdot \frac{\mathbf{r}}{r} \quad (4)$$

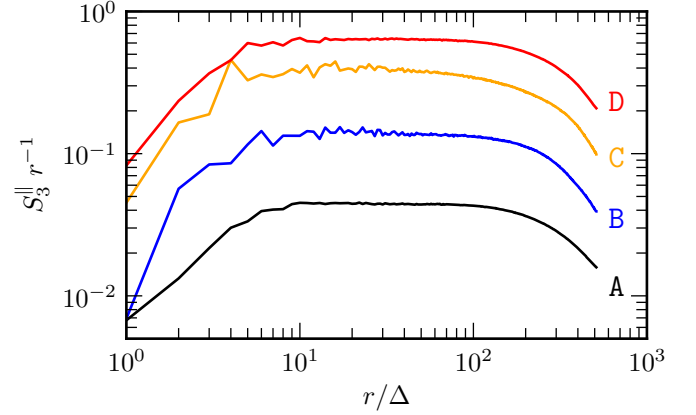


Figure 3. Compensated, third-order, parallel structure function computed for the different models as functions of r/Δ . Note the very good match with the classical $S_3^{\parallel} \sim r$ behaviour.

where \mathbf{r} is a vector of length r and the average is over space and time.

Figure 3 reports the compensated, third-order, parallel structure function, S_3^{\parallel} , as functions of r/Δ , where Δ is the grid spacing. Within the inertial range, classical incompressible turbulence has a precise prediction: the Kolmogorov 4/5-law, for which $\langle (\delta_r v)^3 \rangle = \frac{4}{5} \epsilon r$, where ϵ is the kinetic-energy dissipation rate. This translates into $S_3^{\parallel} \sim \epsilon r$. As shown in the figure, the structure functions are somewhat noisy at small scales, but are consistent with the classical prediction over a wide range of lengthscales, with linear fits showing deviations of $\sim 5\%$, and an increase of ϵ with the driving force.

Although even in the classical compressible case, the 4/5-law is not strictly valid, we can use it to obtain a rough estimate of the turbulent velocity dissipation rate (Porter et al. 2002). We find that ϵ , as measured from S_3^{\parallel} or directly from $\langle (\delta_r v)^3 \rangle$, grows linearly with the Lorentz factor, in contrast with the classical theory, where it is known to be independent of the Reynolds number. This is consistent with the observations that in a relativistic regime the turbulent velocity shows an exponential decay in time (Zrake et al. 2011; Inoue et al. 2011), as opposed to the power-law decay seen in classical compressible and incompressible turbulence.

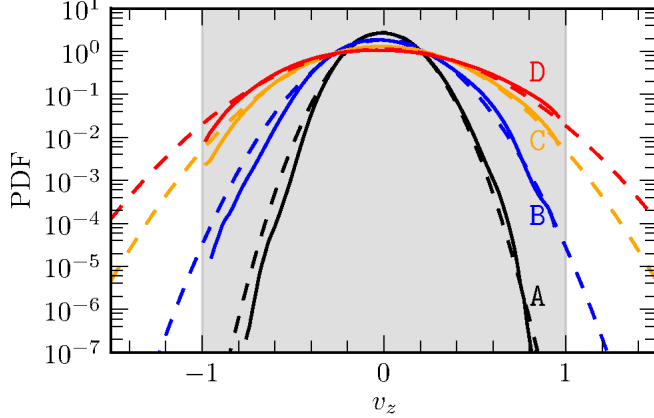
The scaling exponents of the parallel structure functions, ζ_p^{\parallel} have been computed up to $p = 10$ using the extended-self-similarity (ESS) technique (Benzi et al. 1993) and are summarized in Table 1. The errors are estimated by computing the exponents without the ESS or using only the data at the final time. We also show the values as computed using the classical K41 theory, as well as using the estimates by She and Leveque (SL) (She & Leveque 1994) for incompressible turbulence, *i.e.* $\zeta_p^{\parallel} = \frac{p}{9} + 2 - 2(\frac{2}{3})^{p/3}$, and those by Boldyrev (Boldyrev 2002) for Kolmogorov-Burgers supersonic turbulence, *i.e.* $\zeta_p^{\parallel} = \frac{p}{9} + 1 - (\frac{1}{3})^{p/3}$.

Not surprisingly, as the flow becomes supersonic, the high-order exponents tend to flatten out and be compatible with the Boldyrev scaling, as the most singular velocity structures become two-dimensional shock waves. ζ_2^{\parallel} , instead, is compatible with the She-Leveque model even in the supersonic case. This is consistent with the observed scaling of the velocity power spectrum, which presents only small intermittency corrections to the $k^{-5/3}$ scaling. Previous classical studies of weakly compressible (Benzi et al. 2008) and supersonic tur-

Table 1

Scaling exponents of the parallel structure functions computed using the ESS technique and analytical predictions from the KS41, SL and Boldyrev models.

| Model | ζ_1^{\parallel} | ζ_2^{\parallel} | ζ_3^{\parallel} | ζ_4^{\parallel} | ζ_5^{\parallel} | ζ_6^{\parallel} | ζ_7^{\parallel} | ζ_8^{\parallel} | ζ_9^{\parallel} | ζ_{10}^{\parallel} |
|----------|-----------------------|-----------------------|-----------------------|-----------------------|-----------------------|-----------------------|-----------------------|-----------------------|-----------------------|--------------------------|
| K41 | 0.33 | 0.67 | 1 | 1.33 | 1.67 | 2 | 2.33 | 2.67 | 3 | 3.33 |
| SL | 0.36 | 0.70 | 1 | 1.28 | 1.54 | 1.78 | 2.00 | 2.21 | 2.41 | 2.59 |
| Boldyrev | 0.41 | 0.74 | 1 | 1.21 | 1.39 | 1.56 | 1.70 | 1.84 | 1.96 | 2.08 |
| A512 | 0.37 ± 0.01 | 0.70 ± 0.02 | 1 ± 0.02 | 1.27 ± 0.03 | 1.51 ± 0.02 | 1.72 ± 0.03 | 1.89 ± 0.04 | 2.04 ± 0.04 | 2.17 ± 0.03 | 2.27 ± 0.02 |
| B512 | 0.36 ± 0.01 | 0.70 ± 0.03 | 1 ± 0.04 | 1.27 ± 0.05 | 1.50 ± 0.07 | 1.70 ± 0.08 | 1.86 ± 0.12 | 1.99 ± 0.16 | 2.10 ± 0.21 | 2.18 ± 0.26 |
| C512 | 0.37 ± 0.01 | 0.70 ± 0.02 | 1 ± 0.03 | 1.26 ± 0.04 | 1.48 ± 0.05 | 1.68 ± 0.07 | 1.84 ± 0.09 | 1.98 ± 0.11 | 2.09 ± 0.13 | 2.19 ± 0.16 |
| D512 | 0.38 ± 0.005 | 0.71 ± 0.01 | 1 ± 0.03 | 1.25 ± 0.03 | 1.46 ± 0.05 | 1.64 ± 0.07 | 1.79 ± 0.09 | 1.92 ± 0.11 | 2.04 ± 0.14 | 2.14 ± 0.16 |

**Figure 4.** PDFs of the velocity v_z for the different models considered (solid lines). As the forcing is increased, the PDFs flatten, while constrained to be in $(-1, 1)$ (shaded area). Increasingly large deviations from Gaussianity (dashed lines) appear in the relativistic regime.

bulence (Porter et al. 2002) found the scaling exponents to be in very good agreement with the ones of the incompressible case and to be well described by the SL model. This is very different from what we observe even in our subsonic model A, in which the exponents are significantly flatter than in the SL model, suggesting a stronger intermittency correction. This deviation is another important result of our simulations.

One non-classical source of intermittency is the genuinely relativistic constraint that the velocity field cannot be Gaussian as the PDFs must have compact support in $(-1, 1)$. This is shown by the behaviour of the PDFs of v_z and plotted as solid lines in the shaded area of Fig. 4. Clearly, as the Lorentz factor increases, the PDFs become flatter and, as a consequence, the velocity field shows larger deviations from Gaussianity (dashed lines). Stated differently, relativistic turbulence is significantly more intermittent than its classical counterpart.

6. CONCLUSIONS.

Using a series of high-order direct numerical simulations of driven relativistic turbulence in a hot plasma, we have explored the statistical properties of relativistic turbulent flows

with average Mach numbers ranging from 0.4 to 1.7 and average Lorentz factors up to 1.7. We have found that relativistic effects enhance significantly the intermittency of the flow and affect the high-order statistics of the velocity field. Nevertheless, the low-order statistics appear to be universal, *i.e.* independent from the Lorentz factor, and in good agreement with the classical Kolmogorov theory.

We thank M.A. Aloy, P. Cerdá-Durán, A. MacFadyen, M. Obergaulinger and J. Zrake for discussions. The calculations were performed on the clusters at the AEI. Partial support comes from the DFG grant SFB/Transregio 7 and by “CompStar”, a Research Networking Programme of the ESF.

REFERENCES

- Benzi, R., Biferale, L., Fisher, R., Kadanoff, L., Lamb, D., & Toschi, F. 2008, *Phys. Rev. Lett.*, 100, 1
- Benzi, R., Ciliberto, S., Tripiccone, R., Baudet, C., Massaioli, F., & Succi, S. 1993, *Phys. Rev. E*, 48, 29
- Boldyrev, S. 2002, *The Astrophysical Journal*, 569, 841
- Font, J. A. 2008, *Living Rev. Relativ.*, 6, 4
- Hawke, I. 2001, PhD thesis, University of Cambridge
- Inoue, T., Asano, K., & Ioka, K. 2011, *Astrophys. J.*, 734, 77
- Kolmogorov, A. N. 1991, *Proceedings of the Royal Society A: Mathematical, Physical and Engineering Sciences*, 434, 9
- Porter, D., Pouquet, A., & Woodward, P. 2002, *Phys. Rev. E*, 66, 1
- Radice, D., & Rezzolla, L. 2012, *Astronomy and Astrophysics*, in press, arXiv:1206.6502
- Rezzolla, L., & Zanotti, O. 2002, *Phys. Rev. Lett.*, 89, 114501
- She, Z., & Leveque, E. 1994, *Phys. Rev. Lett.*, 72, 336
- Suresh, A., & Huynh, H. T. 1997, *Journal of Computational Physics*, 136, 83
- Toro, E. F. 1999, *Riemann Solvers and Numerical Methods for Fluid Dynamics* (Springer-Verlag)
- Zhang, W., MacFadyen, A., & Wang, P. 2009, *Astrophys. J.*, 692, L40
- Zrake, J., MacFadyen, A., McEnery, J. E., Racusin, J. L., & Gehrels, N. 2011, 102–105
- Zrake, J., & MacFadyen, A. I. 2012, *Astrophys. J.*, 744, 32